Check for updates

Original Research Article

International journal of spray and combustion dynamics

International Journal of Spray and Combustion Dynamics
2018, Vol. 10(4) 380–392
© The Author(s) 2018
Article reuse guidelines:
sagepub.com/journals-permissions
DOI: 10.1177/1756827718789066
journals.sagepub.com/home/scd
SAGE

Assessing the stochastic error of acoustic scattering matrices using linear methods

Luck Peerlings[1], Friedrich Bake[2], Susann Boij[1] and Hans Bodén[1]

Abstract

To be able to compare the measured scattering matrices with model predictions, the quality of the measurements has to be known. Uncertainty analyses are invaluable to assess and improve the quality of measurement results in terms of accuracy and precision. Linear analyses are widespread, computationally fast and give information of the contribution of each error source to the overall measurement uncertainty; however, they cannot be applied in every situation. The purpose of this study is to determine if linear methods can be used to assess the quality of acoustic scattering matrices.

The uncertainty in measured scattering matrices is assessed using a linear uncertainty analysis and the results are compared against Monte-Carlo simulations. It is shown that for plane waves, a linear uncertainty analysis, applied to the wave decomposition method, gives correct results when three conditions are satisfied. For higher order mode measurements, the number of conditions that have to be satisfied increases rapidly and the linear analysis becomes an unsuitable choice to determine the uncertainty on the scattering matrix coefficients. As the linear uncertainty analysis is most suitable for the plane wave range, an alternative linear method to assess the quality of the measurements is investigated. This method, based on matrix perturbation theory, gives qualitative information in the form of partial condition numbers and the implementation is straightforward. Using the alternative method, the measurements of higher order modes are analyzed and the observed difference in the measured reflection coefficients for different excitation conditions is explained by the disparity in modal amplitudes.

Keywords

Uncertainty analysis, higher order modes, sensitivity analysis, partial condition numbers, in-duct acoustics

Date received: 30 March 2017; accepted: 22 June 2018

1. Introduction

The interest in measuring the scattering matrix for higher order modes in ducts with flow has increased recently and measurements have been made on rectangular and circular ducts.[1–3] One of the advantages of including higher order modes is the possibility to increase the frequency range in which measurements can be made. Recently, new models are proposed to describe the wave propagation constants for plane waves and higher order modes in turbulent pipe flows.[3,4] To verify these models, it is necessary to perform precise acoustic measurements where the uncertainty in the measurement data has been assessed.

For plane waves, the errors that can arise using the two-microphone methods are well known and are described qualitatively in Åbom and Bodén,[5] Bodén,[6] and Hudde and Letens,[7] with generalized optimality conditions described in Åbom and Bodén[5] and Bodén.[6] Methods to reduce systematic errors are described in Katz,[8] Boonen et al.,[9] Dickens et al.,[10]

[1]KTH Royal Institute of Technology, Department of Aeronautical and Vehicle Engineering, Marcus Wallenberg Laboratory for Sound and Vibration, Stockholm, Sweden
[2]German Aerospace Center, Institute of Propulsion Technology, Engine Acoustics, Berlin, Germany

Corresponding author:
Luck Peerlings, KTH Royal Institute of Technology, Department of Aeronautical and Vehicle Engineering, Marcus Wallenberg Laboratory for Sound and Vibration, Teknikringen 8, 10044 Stockholm, Sweden.
Email: luck@kth.se

Creative Commons Non Commercial CC BY-NC: This article is distributed under the terms of the Creative Commons Attribution-NonCommercial 4.0 License (http://www.creativecommons.org/licenses/by-nc/4.0/) which permits non-commercial use, reproduction and distribution of the work without further permission provided the original work is attributed as specified on the SAGE and Open Access pages (https://us.sagepub.com/en-us/nam/open-access-at-sage).

and Gibiat and Laloë[11] and techniques to quantitatively assess the measurement uncertainty have been described in Schultz et al.[12]

In comparison, investigations of the errors in measurements with higher order modes have not received the same attention. Efforts to reduce systematic errors and improve the accuracy of the measurement results for higher order modes have been recently published. For example, Sack and Åbom investigated the sensitivity of the modal decomposition results with respect to sensor and source positions.[13] Suzuki and Day investigated the use of different algorithms to decompose the sound field in the various wave components.[14] The lack of design guidelines can partially be explained by the fact that the number of free parameters are significantly increased compared to that of the two-microphone method for plane waves, making it difficult to create generalized optimality conditions, such as those derived by Bodén and Åbom.[5,6]

To compare model predictions and measurements with each other, the uncertainty in the measurements has to be known to make definitive statements on the agreement. Also, the uncertainty itself can be used to assess the quality of the measurements and determine the contribution of individual error sources, helpful when improving the measurements.

Two methods are often used to determine the uncertainty of measurements. The first is the multi-variate analysis,[15] which is based on a linear approximation of the equation describing the relation between the measured variables, for example the transfer functions, and the quantity of interest, such as the scattering coefficients. The second method, the Monte-Carlo method,[15] uses a numerical approach where the inputs are considered as random variables and a set of measurement samples are generated based on the statistical properties of the inputs. The quantity of interest is calculated for each set of input samples and the resulting statistical properties of the outputs can be calculated.

The benefit of the Monte-Carlo method is that it includes the effect of non-linear error propagation; however, the drawback of the method is the computational time. On the other hand, the multi-variate analysis is based on an analytical approach and is significantly faster; however, it can only take into account linear error propagation.

The purpose of this study is to investigate if a linear multi-variate approximation is sufficient to quantify the uncertainty of higher order modes measurements. A subject closely related to the linear uncertainty analysis is the theory of matrix perturbations. With methods from matrix perturbation theory, it is possible to determine the sensitivity of the wave decomposition method to input perturbations using analytical methods. Such an approach is beneficial in the process of designing new setups as the solution is straightforward to implement and computationally fast, but it only gives qualitative information.

The linear uncertainty analysis will be investigated for higher order mode scattering matrices using the multi-microphone method[16] in a generalized way. Only solutions to the linear equations will be considered, without iterative refinement, and the sound fields are assumed to be harmonic in time.

2. Scattering matrix

The scattering matrix is a concept, used in various branches of physics, such as electronics where it describes the relation between electrical quantities at different electric lines of an electric network.[17,18] In an analogous way, the scattering matrix for acoustic networks relates the acoustic fields at different physical ports to each other. In the scattering matrix representation, the sound fields are described by propagating waves and the scattering matrix relates the incident to the outgoing waves from each port.

Considering harmonic acoustic fields, with a time dependence of $e^{i\omega t}$ where ω is the angular frequency, the acoustic field within an acoustic wave guide can be described as an infinite sum of modes, if the cross-sectional area and the flow profile within the duct are independent of the axial direction. The spatial dependency of the pressure field in the axial, x-direction and cross-sectional directions, y and z, can then be written as

$$p(x,y,z,\omega) = \sum_{l=0}^{\infty} p_l^+ \psi_l(M,y,z) e^{-ik_l(M,\omega)x} + p_l^- \psi_l(M,y,z) e^{ik_l(M,\omega)x} \quad (1)$$

The modal amplitudes of mode l propagating in the positive and negative x-direction are given by p_l^+ and p_l^- respectively. The propagation direction does not have to coincide with the direction of the mean flow. The mean flow is characterized by the Mach-number M, which has no spatial dependency and is defined as the mean flow velocity normalized by the speed of sound, c_0, in the medium. The specific mode shape is given by ψ_l and its corresponding wave number by k_l. The various modes are ordered by their cut-on frequency[19] and the number of modes used to describe the sound field is truncated to the L modes that significantly contribute to the sound field far away from irregularities in the duct. The modes are propagating when the real part of the free-field wave number, given by $k_0 = \omega/c_0$, is larger than the real part of the cut-on wave number of the mode l, $\Re(k_0) > \Re(k_l^c)$. The wave-numbers k_l can be analytically or numerically determined.[20–22]

For waves in circular and rectangular ducts, neglecting losses in the fluid and at the wall and including the effect of uniform mean flow, the axial wave number for mode l is given by

$$k_l = k_0 \frac{M \pm \sqrt{1-(1-M^2)k_l^{c2}/k_0^2}}{1-M^2} \tag{2}$$

with k_0 the free field wave number, given by ω/c_0 and k_l^c the cut-on wavenumber for the mode l. The plus-minus sign indicates whether the wave is travelling in the direction of the flow (+) or against the flow (-). For rectangular ducts, the cut-on wavenumbers are given by

$$k_l^c = \sqrt{\left(\frac{m_l\pi}{b}\right)^2 + \left(\frac{n_l\pi}{h}\right)^2}, \quad n_l, m_l \in \mathbb{N} \tag{3}$$

where b is the width of the duct and h the height of the duct. The corresponding modeshapes are given by

$$\psi_l(y,z) = \cos\left(\frac{m_l\pi}{b}y\right)\cos\left(\frac{n_l\pi}{h}z\right) \tag{4}$$

For waves in circular ducts, the cut-on wave numbers are given by the solutions to the equation

$$J'_{m_l}(k_l^c) = 0, \quad m_l \in \mathbb{N} \tag{5}$$

where J'_m is the derivative of the Bessel function of the first kind of order m. The corresponding mode shapes are given by

$$\psi_l(r,\theta) = \exp(im\theta)J_m(k_l r) \tag{6}$$

where r is the radius from the center of the duct and θ the angle in the cross sectional plane of the duct.

Now consider a device which has N number of physical ports. At each port, the sound field can be decomposed using equation (1) and the relation between the waves propagating to and away from the object is then given by the scattering matrix $\boldsymbol{S}$.

When an equal number of modes are considered to be incident on and travelling away from the object, $\boldsymbol{S} \in \mathbb{C}^{\mathcal{L}x\mathcal{L}}$, with $\mathcal{L}$ the total number of modes propagating to or away from the object.

The relation between the acoustic field propagating to and away from the object is given by

$$\boldsymbol{p}^- = \boldsymbol{S}\boldsymbol{p}^+ \tag{7}$$

where the vectors $\boldsymbol{p}^+$ and $\boldsymbol{p}^-$ are a concatenation of modal amplitudes respectively travelling towards and away from the object from all the N ports.

To simplify the notation, from here onward the notation $\boldsymbol{p}^\pm$ will be used to indicate that the relation hold for both the waves traveling to, $\boldsymbol{p}^+$, and away, $\boldsymbol{p}^-$, from the object. The vectors $\boldsymbol{p}^\pm$ are given by

$$\boldsymbol{p}^\pm = \begin{bmatrix} \boldsymbol{p}_1^\pm & \dots & \boldsymbol{p}_n^\pm & \dots & \boldsymbol{p}_N^\pm \end{bmatrix}^T \in \mathbb{C}^{\mathcal{L}x1} \tag{8}$$

where $\boldsymbol{p}_n^\pm \in \mathbb{C}^{\mathcal{L}x1}$, with L the number of incident or scattered modes propagating in a specific duct n

$$\boldsymbol{p}_n^\pm = \begin{bmatrix} p_1^\pm & \dots & p_l^\pm & \dots & p_L^\pm \end{bmatrix}^T \tag{9}$$

The scattering matrix can be determined from experimental or numerical data by solving

$$\boldsymbol{P}^- = \boldsymbol{S}\boldsymbol{P}^+ \tag{10}$$

where the matrices $\boldsymbol{P}^\pm$ are a concatenation of the $\mathcal{K}$ measured vectors $\boldsymbol{p}^\pm$

$$\boldsymbol{P}^\pm = \begin{bmatrix} \boldsymbol{p}_1^\pm \dots \boldsymbol{p}_k^\pm \dots \boldsymbol{p}_\mathcal{K}^\pm \end{bmatrix}, \quad \boldsymbol{P}^\pm \in \mathbb{C}^{\mathcal{L}x\mathcal{K}} \tag{11}$$

To determine the scattering matrix using equation (10), at least $\mathcal{K} \geq \mathcal{L}$ linearly independent incident and reflected sound fields have to be measured, such that the $\text{rank}(\boldsymbol{P}^\pm) = \mathcal{L}$.

The vectors $\boldsymbol{p}_n^\pm$ describing the waves that are present in each duct n can be determined using the so called wave-decomposition method. The pressure at different positions is measured, and using the modal representation, equation (1), a linear system of equations can be constructed

$$\boldsymbol{\Psi}_n \begin{bmatrix} \boldsymbol{p}_n^+ \\ \boldsymbol{p}_n^- \end{bmatrix} = \begin{bmatrix} p_i \\ \vdots \\ p_I \end{bmatrix} \tag{12}$$

where p_i is the pressure measured at the position $\boldsymbol{x}_i = [x_i, y_i, z_i]$ in the duct. The matrix $\boldsymbol{\Psi}_n$ relates the pressures at a certain position in duct n with the modal amplitudes and is given by

$$\boldsymbol{\Psi}_n = \begin{bmatrix} \boldsymbol{\Psi}_1 & \dots & \boldsymbol{\Psi}_i & \dots & \boldsymbol{\Psi}_I \end{bmatrix}, \quad \Psi \in \mathbb{C}^{\text{Ix}2\mathcal{L}} \tag{13}$$

where I is the number of microphone positions. The rows in $\boldsymbol{\Psi}$ are given by

$$\boldsymbol{\Psi}_i = \begin{bmatrix} \psi_1(M, y_i, z_i)e^{ik_1(M)x_i} \\ \vdots \\ \psi_l(M, y_i, z_i)e^{ik_l(M)x_i} \\ \psi_1(-M, y_i, z_i)e^{-ik_1(-M)x_i} \\ \vdots \\ \psi_l(-M, y_i, z_i)e^{-ik_l(-M)x_i} \end{bmatrix}^T \tag{14}$$

To solve the system (equation (12)), the pressure should be measured at $I \geq 2L$ different positions and $\text{rank}(\boldsymbol{\Psi}_n) = 2L$.

3. Linear uncertainty analysis

The elements of the scattering matrix $\boldsymbol{S}$, also called scattering coefficients, are complex variables relating the amplitude and phase of the in-going to the outgoing modes. When performing a measurement, there is always an uncertainty associated with the measured quantities, which will lead to an uncertainty in the obtained scattering coefficients.

Some measured quantities and the scattering coefficients are complex and to describe their uncertainty, they are decomposed in the real part u and the imaginary part v, $\boldsymbol{z} = \begin{bmatrix} u & v \end{bmatrix}^T \in \mathbb{R}^{2x1}$. If the real and imaginary parts of z are normally distributed, the joint probability density function can be fully described by the variance of the real and imaginary part and the covariance between them[23,24]

$$p(u, v) = \frac{1}{2\pi\sqrt{\det \boldsymbol{R}_{zz}}} \exp\left(-\frac{1}{2}\boldsymbol{z}^T \boldsymbol{R}_{zz}^{-1} \boldsymbol{z}\right) \tag{15}$$

where the covariance matrix is given by $\boldsymbol{R}_{zz}$

$$\text{cov}(z) = \boldsymbol{R}_{zz} = \text{E}\left[(\boldsymbol{z} - \boldsymbol{\mu}_z)(\boldsymbol{z} - \boldsymbol{\mu}_z)^T\right] \tag{16}$$

where $\text{E}[\cdot]$ is the expectation operator and $\boldsymbol{\mu}_z = \text{E}(\boldsymbol{z})$.

The purpose of an uncertainty analysis is to determine the statistical properties of the parameters of interest, such as the elements of $\boldsymbol{S}$ as function of the statistical properties of the known parameters, such as the measured parameters p_i.

Consider a general function $\boldsymbol{y} = f(\boldsymbol{x})$, which represent the relationship between the parameters of interest $\boldsymbol{y}$ and the measured parameters $\boldsymbol{x}$. If this relationship can be considered linear in the neighbourhood of $\boldsymbol{x}$, for which the size is proportional to the size of covariances of $\boldsymbol{x}$, a linear multi-variate uncertainty analysis can be used to relate the covariance matrices of the known parameters $\boldsymbol{x}$ to the covariance matrices of the parameters of interest $\boldsymbol{y}$.

The linear multi-variate uncertainty analysis is based on a first-order Taylor's expansion of the function f. It is possible to take into account higher order terms in the Taylor expansion and include higher order statistical moments into the analysis,[25] however, the computations quickly become cumbersome.

Considering only the first-order Taylor expansion of $\boldsymbol{y} = f(\boldsymbol{x})$, the deviation $\widehat{\boldsymbol{y}}_k$ of a single (complex) parameter of interest, $\boldsymbol{y}_k$ from its true value $\boldsymbol{y}_k^0$, is given by

$$\widehat{\boldsymbol{y}}_k = \boldsymbol{y}_k - \boldsymbol{y}_k^0 \in \mathbb{R}^{2x1} \tag{17}$$

This deviation, or error, can be expressed as function of the deviations of the measured parameters from their true values using the first order Taylor expansion of $\boldsymbol{y} = f(\boldsymbol{x})$ for each complex element $\boldsymbol{x}_i$

$$\widehat{\boldsymbol{y}}_k \approx \sum_i^N \boldsymbol{J}_i^k \left(\boldsymbol{x}_i - \boldsymbol{x}_i^0\right) \in \mathbb{R}^{2x1} \tag{18}$$

where $\boldsymbol{J}_i^k$ is the complex Jacobian matrix of the kth output value w.r.t to i-th input variable evaluated at the position $\boldsymbol{x}_i^0 \in \mathbb{R}^{2x1}$ and given by

$$\boldsymbol{J}_i^k = \begin{bmatrix} \dfrac{\partial}{\partial u_k}\boldsymbol{x}_i & \dfrac{\partial}{\partial v_k}\boldsymbol{x}_i \end{bmatrix} \in \mathbb{R}^{2x2} \tag{19}$$

The covariance matrix of the error of the parameter of interest is given by

$$\text{cov}\,\widehat{\boldsymbol{y}}_k = \text{E}\left[\left(\boldsymbol{y}_k - \boldsymbol{\mu}_{yk}\right)\left(\boldsymbol{y}_k - \boldsymbol{\mu}_{yk}\right)^T\right] \in \mathbb{R}^{2x2} \tag{20}$$

where $\boldsymbol{\mu}_{yk} = \text{E}\left[\boldsymbol{y}_k\right]$. Using equation (18) it can be written as

$$\text{cov}\,\widehat{\boldsymbol{y}}_k \approx \sum_i^N \sum_j^N \boldsymbol{J}_i^k(f)\,\text{cov}(\boldsymbol{x}_i, \boldsymbol{x}_j)\left[\boldsymbol{J}_j^k(f)\right]^T \tag{21}$$

where the cross-covariance $\text{cov}(x_i, x_j)$ is given by

$$\text{cov}(\boldsymbol{x}_i, \boldsymbol{x}_j) = \text{E}\left[(\boldsymbol{x}_i - \boldsymbol{\mu}_{x_i})(\boldsymbol{x}_j - \boldsymbol{\mu}_{x_j})^T\right] \tag{22}$$

An advantage of the linear analysis is that the contribution from each error source to the overall uncertainty can be easily calculated which is beneficial in the design and improvement of experimental setups.

If the relationship $f(\boldsymbol{z})$ is not linear in the neighbourhood of $\boldsymbol{z}$, other methods, such as the Monte-Carlo method, have to be used to determine the statistical parameters of $\boldsymbol{y}$. Using the Monte-Carlo method, numerically many 'draws' from a single measurement are simulated based on the statistical properties of the input variables. From the draws, the mean value and statistical parameters of the output values are calculated.[15] With this method, the statistical properties can be calculated for an arbitrary relation between the input and output parameters, but it is computationally heavy.

As the linear uncertainty analysis is a useful tool to express and analyze the uncertainty, the question arises when such an analysis is appropriate without performing a validation against a Monte-Carlo simulation. By analyzing the sources of non-linearity when

determining the N-port scattering matrix, estimators can be derived to determine if a linear analysis gives correct results.

There are three sources of non-linearity when calculating the scattering matrix. Two are related by the matrix inversion needed to obtain the solution to equations (10) and (12). The third source of non-linearity is the relationships of the matrix elements in $\boldsymbol{\Psi}$ with respect to their arguments.

The first source of non-linearity that we consider are perturbations of the elements of $\boldsymbol{\Psi}$. Consider the Taylor expansion of the matrix

$$\boldsymbol{\Psi}(a+\epsilon) = \boldsymbol{\Psi} + \frac{\partial \boldsymbol{\Psi}}{\partial a}\epsilon + \frac{1}{2}\frac{\partial^2 \boldsymbol{\Psi}}{\partial a^2}\epsilon^2 + \mathcal{O}(\epsilon^3) \tag{23}$$

where a and ϵ represent any input parameter and its error, respectively. The condition to have linear error propagation is that all the second and higher order terms have to be much smaller than the first-order terms

$$\left\| \left[\epsilon \left(\frac{1}{2}\frac{\partial^2 \boldsymbol{\Psi}}{\partial a^2} \right) + \mathcal{O}(\epsilon^2) \right] \oslash \left(\frac{\partial \boldsymbol{\Psi}}{\partial a} \right) \right\|_\infty << 1 \tag{24}$$

where $\oslash$ represents element wise division. The above condition has to be satisfied for all uncertain input parameters to ensure linear error propagation.

The second source of non-linearity is the method used to solve the wave decomposition equation (12). The solution is obtained by pre-multiplying the equations by a Moore–Penrose pseudo-inverse $\boldsymbol{\Psi}^\dagger$, for which small perturbations to $\boldsymbol{\Psi}$ could lead to non-linear perturbations on the inverse. In general, the pseudo-inverse of a perturbed matrix is non-continuous[26]

$$\lim_{\epsilon \to 0} (\boldsymbol{A} + \epsilon \boldsymbol{B})^\dagger \neq \boldsymbol{A}^\dagger \tag{25}$$

However, in the special case that the perturbations on matrix $\boldsymbol{A}$ are acute,[26] that is, the perturbations do not change the rank of $\boldsymbol{A}$, $\mathcal{R}(\boldsymbol{A}) = \mathcal{R}(\boldsymbol{A} + \epsilon \boldsymbol{B})$, the matrix inverse is continuous and can be approximated by a Taylor series.[27]

Consider now the case for the matrix $\boldsymbol{\Psi}$. If the perturbations are small and acute, then the perturbation to the matrix can be written as $\epsilon \boldsymbol{E}$ by neglecting the second order terms in equation (23), with

$$\boldsymbol{E} = \frac{\partial \boldsymbol{\Psi}}{\partial a} \tag{26}$$

and the pseudo-inverse can be approximated by

$$(\boldsymbol{\Psi} + \epsilon \boldsymbol{E})^\dagger = \Psi^\dagger + \sum_{k=1}^{\infty} (-1)^k \left(\boldsymbol{\Psi}^\dagger E \right)^k \boldsymbol{\Psi}^\dagger \epsilon^k \tag{27}$$

for $\|\epsilon \boldsymbol{\Psi}^\dagger E\| < 1$, to have the series converge. Comparing the size of the second order term with the first-order term of equation (27), with a suitable norm

$$\|\epsilon \boldsymbol{\Psi}^\dagger E\| << 1 \tag{28}$$

must be satisfied to ensure that the inversion process is linear. A more conservative but insightful bound is obtained by considering a determined set of equations and using the two-norm. Equation (28) can then be rewritten as

$$\frac{\|\epsilon \boldsymbol{E}\|_2}{||\boldsymbol{\Psi}\|_2} \kappa(\boldsymbol{\Psi}) << 1 \tag{29}$$

where $\kappa(\Psi)$ is the condition number of the matrix . The bound shows that even when the relative perturbations on the matrix $\boldsymbol{\Psi}$ are small, they can still lead to a non-linear contribution to the inverse of the matrix through a badly conditioned matrix $\boldsymbol{\Psi}$.

The third source of non-linearity that can be identified is the method used to solve for the scattering matrix, equation (10). It is also solved by pre-multiplying the equation with $\boldsymbol{P}^{+\dagger}$ and the above reasoning holds as well for this source. It becomes clear from equation (29), that the condition number of $\boldsymbol{P}^+$ has to be small to have a linear error propagation. Therefore, when measuring the scattering matrix, acoustic fields for which the columns of $\boldsymbol{P}^+$ are orthogonal to each other and having a similar magnitude should be used. One way to realize this is to excite only one mode at a particular port for each measurement in equation (11) and have non-reflective boundary conditions for all the other modes at the terminations of each port.

To apply the linear uncertainty analysis, both conditions (24) and (28), should hold for any uncertain input parameter. When higher order modes are cut-on, the number of necessary conditions increases rapidly and it becomes cumbersome to keep track of all the conditions. Unfortunately no specific sets of conditions can be identified which are mutually exclusive and thus all the conditions have to be satisfied to have linear error propagation. Only when plane waves are present, some general statements can be made if a linear uncertainty analysis can be applied.

In the case of plane waves three parameters play a role in the wave decomposition, which are the axial position of the microphone, the Mach number and the free field speed of sound. With the help of equation (24), the linearity conditions for these three parameters can be derived.

The first condition is with respect to the error in the microphone distance

$$\left\| \frac{\epsilon_x k_0}{2} \frac{M+1}{1-M^2} \right\| << 1 \tag{30}$$

Herein ϵ_x is the error in the microphone distance. The second condition is with respect to the error in the Mach number ϵ_M and is given by

$$\left\| \frac{\epsilon_M}{2} \left[\frac{ik_0 x}{(M \pm 1)^2} - \frac{2}{(M \pm 1)} \right] \right\| << 1 \qquad (31)$$

The third condition is with respect to the error affecting the free field wave number, which is related to the speed of sound. The speed of sound can be estimated using $c_0 = \sqrt{\gamma R T}$, where γ is the ratio of specific heats, R the gas constant of the medium and T the temperature of the gas. Considering the uncertainty in the temperature ϵ_T the condition that has to be satisfied can be written as

$$\left\| \frac{\epsilon_T}{2} \left[\frac{i\omega x(1+M)}{2T\sqrt{\gamma R T}(M^2-1)} - \frac{3}{2T} \right] \right\| << 1 \qquad (32)$$

It can be seen that the ratios in equations (30), (31) and (32) increase with frequency and therefore, there will be an upper frequency limit where the linear uncertainty analysis will not be valid anymore. All these conditions have to be satisfied to ensure that the error in the wave decomposition process is linear. As the solution to the wave decomposition equation (12) is linear with respect to the measured pressure $\boldsymbol{p}$, the error of $\boldsymbol{p}$ will propogate linearly to the amplitudes of the propagating waves.

4. Perturbation theory

The linear multi-variate analysis is an effective method to determine the uncertainty, but as argued in the previous sections, it becomes difficult to correctly determine the uncertainty using linear methods when higher order modes are present. In addition, even though the linear uncertainty analysis is computationally fast, the implementation can be cumbersome. On the other hand, when designing a setup, the use of Monte-Carlo methods to estimate the uncertainty could be too time-consuming.

An alternative way to assess the influence of stochastic errors on the measurements can be done using condition numbers. These condition numbers can be computed from the singular value decomposition and matrix norms of the linear system, which are straightforward to calculate using numerical techniques. Using condition numbers, the sensitivity of the measurement results to perturbations (errors) can be examined to obtain a qualitative understanding and can be of interest when designing or analyzing a setup.

In the field of computer science and scientific computing, the response of linear systems to perturbations is actively studied and the following section is a recapitulation of material that can be found in Stewart and Sun,[26] Geurts,[28] Arioli et al.,[29] and Baboulin et al.[30]

To determine the response of linear systems to small perturbations, the set of linear equations are considered as a map of one linear space to another linear space. As an example, equation (12) is given by

$$\boldsymbol{\Psi}_n \begin{bmatrix} \boldsymbol{p}_n^+ \\ \boldsymbol{p}_n^- \end{bmatrix} = \begin{bmatrix} p_i \\ \vdots \\ p_I \end{bmatrix}$$

which can be interpreted as a map of the data space, spanned by the model, $\boldsymbol{\Psi}_n$, and measurements, $[p_i \ldots p_I]$, to the solution space spanned by $\left[\boldsymbol{p}_n^+ \; \boldsymbol{p}_n^-\right]^T$. The sensitivity of the system of equations can be determined by analyzing the results of small perturbations in the data space to changes in the solution space. The ratio between the size of the perturbations on the solution space to the perturbations in the data space is defined as the condition number of the system of equations. As the data space consists of both the model and measurements and the solution and data spaces are multi-dimensional, the definition of the size of a perturbation is not unique and condition numbers can be defined in many ways.

Consider a map g, which maps an m-dimensional data space to a n dimensional solution space with $n \leq m$, $g: \mathbb{R}^m \rightarrow \mathbb{R}^n$. The condition number of the system gives a measure of the sensitivity of the map $g(\boldsymbol{y}_0)$ to perturbations in the data space $\boldsymbol{y}_0$.

The condition number of the system is defined by[29,30]

$$K(\boldsymbol{y}_0) = \lim_{\delta \rightarrow 0} \sup_{0 < \|\boldsymbol{y}_0 - \boldsymbol{y}\|_{\mathcal{D}} \leq \delta} \frac{\|g(\boldsymbol{y}_0) - g(\boldsymbol{y})\|_{\mathcal{S}}}{\|\boldsymbol{y}_0 - \boldsymbol{y}\|_{\mathcal{D}}} \qquad (33)$$

where sup denotes the supremum of the subset of numbers, $\|.\|_{\mathcal{D}}$ is the norm used in the data space and $\|.\|_{\mathcal{S}}$ the norm used in the solution space to measure the size of a vector. The supremum of a set is the smallest upper bound of a set, which does not have to be a member of the set itself. The supremum is a similar concept as the maximum of a set; however the supremum is unique and always exists. The condition number of the system represents an asymptotic sensitivity to infinitesimal perturbations and is dependent on the choice of the norms for the data and solution space. The relative condition number is defined as

$$K^{(rel)}(\boldsymbol{y}_0) = K(\boldsymbol{y}_0)\|\boldsymbol{y}_0\|_{\mathcal{D}} / \|g(\boldsymbol{y}_0)\|_{\mathcal{S}} \qquad (34)$$

In the current study, the map is given by the solution to an (over)-determined system of linear equations (12) and (10). A condition number that is sometimes used to express the sensitivity of a solution to linear equations $\boldsymbol{A}\boldsymbol{x} = \boldsymbol{b}$ is given by

$$\kappa(\boldsymbol{A}) \equiv \|\boldsymbol{A}\|_2 \, \|\boldsymbol{A}^{-1}\|_2 \qquad (35)$$

where $\|\cdot\|_2$ is the two-norm. This condition number gives an upper bound for the sensitivity of the solution to perturbations to the system. Equation (35) is a special case of equation (34), when a determined set of equations is considered, only $\boldsymbol{A}$ is perturbed and the perturbations in the data space and solution space are measured by the two-norm.[28,31]

In general, equations (12) and (7) are over-determined systems, which are more prone to ill-conditioning as the sensitivity can scale with the square root of the condition number κ, as defined by equation (35).[31–33] Therefore, equation (35) is not the optimal way to determine the sensitivity of these systems of equations. Furthermore, the above condition number only gives information on the size of the perturbations on the solution vector $\boldsymbol{x}$ and not a specific element x_i of the solution vector.

Arioli et al.[29] give methods to determine the condition numbers for over-determined systems of equations. The theorem presented by Arioli et al.,[29] (Theorem 1) allows deriving the exact condition number in the form of equation (33) under special conditions. The condition numbers are obtained for specific elements of the solution vector $\boldsymbol{x}$ and for perturbations on $\boldsymbol{A}$ and/or $\boldsymbol{b}$.

In the following, the theorem and a minimum amount of theory is introduced to understand the theorem. The interested reader is referred to Arioli et al.[29] and Baboulin et al.[30] The results are obtained for maps in the real domain $\mathbb{R}$, but it is assumed that the results also hold for the complex domain $\mathbb{C}$ as the system of equations are continuous in the complex domain and the perturbations are assumed to be acute, implying that the complete system is continuous and thus Fréchet-differentiable.

Consider a map g of a linear least squares solution $\min_{x\in\mathbb{R}^n}\|\boldsymbol{A}\boldsymbol{x}-\boldsymbol{b}\|_2$, which is projected on to a k dimensional space $\boldsymbol{L}^T\boldsymbol{x},\ L\in\mathbb{R}^{nxk}$. The map is given by

$$g\ :\ \mathbb{C}^{mxn}\times\mathbb{C}^m\rightarrow\mathbb{C}^k,\qquad \boldsymbol{A},\boldsymbol{b}\mapsto g(\boldsymbol{A},\boldsymbol{b})=\boldsymbol{L}^T\boldsymbol{x}(\boldsymbol{A},\boldsymbol{b})=\boldsymbol{L}^T(\boldsymbol{A}^T\boldsymbol{A})^{-1}\boldsymbol{A}^T\boldsymbol{b} \tag{36}$$

The projection on the k dimensional space allows the determination of the condition number for a specific element of the solution vector $\boldsymbol{x}$, by choosing $\boldsymbol{L}$ such that it is a column of the identity matrix.

Values, as opposed to bounds, of the condition number of the above system can be derived, when suitable norms for the solution and data space are taken. For the solution space the two-norm is used. For the data space, the following norm is used

$$\|(\boldsymbol{A},\boldsymbol{b})\|_F=\sqrt{\alpha^2\|\boldsymbol{A}\|_F^2+\beta^2\|\boldsymbol{b}\|_2^2},\quad \alpha,\beta>0\in\mathbb{R} \tag{37}$$

where $\|\cdot\|_F$ stands for the Frobenius norm and $\|\cdot\|_2$ for the two-norm. The Frobenius norm is given by

$$\|\boldsymbol{A}\|_F=\sqrt{\text{trace}[\boldsymbol{A}^*\boldsymbol{A}]} \tag{38}$$

where $\boldsymbol{A}^*$ denotes the conjugate transpose of $\boldsymbol{A}$. With the above norm, it is possible to estimate the effect of perturbations on $\boldsymbol{A}$ and $\boldsymbol{b}$ separately. For values of $\alpha\rightarrow\infty$, the condition number of the problem is obtained where mainly $\boldsymbol{b}$ is perturbed and for values of $\beta\rightarrow\infty$ the condition number of the problem is obtained where mainly $\boldsymbol{A}$ is perturbed.[30] The condition numbers as defined in equation (33) can then be computed with the theorem[29] (Theorem 1), given by:

Theorem 1. Let $\boldsymbol{A}=\boldsymbol{U}\boldsymbol{V}^T$ *be the thin singular value decomposition of* $\boldsymbol{A}$, *with* $=\text{diag}(\sigma_i)$ *and* $\sigma_1\geq\sigma_2\ldots\geq\sigma_n\geq 0$. *The absolute condition number of* $g(\boldsymbol{A},\boldsymbol{b})=\boldsymbol{L}^T\boldsymbol{x}(\boldsymbol{A},\boldsymbol{b})$, *where the norm of the solution space is the Frobenius norm, is given by*

$$K(\boldsymbol{L}^T\boldsymbol{x})=\|\boldsymbol{S}\boldsymbol{V}^T\boldsymbol{L}\|_2 \tag{39}$$

where $\boldsymbol{S}\in\mathbb{R}^{nxn}$ *is the diagonal matrix with diagonal elements*

$$S_{ii}=\sigma_i^{-1}\sqrt{\frac{\sigma_i^{-2}\|\boldsymbol{r}\|_2^2+\|\boldsymbol{x}\|_2^2}{\alpha^2}+\frac{1}{\beta^2}} \tag{40}$$

where $\boldsymbol{r}$, *the residual, is given by* $\boldsymbol{r}=\boldsymbol{A}\boldsymbol{x}-\boldsymbol{b}$.

The thin singular value decomposition is given by the singular value decomposition where only the column vectors of U and the row vectors of V^T are calculated that correspond to the non zero singular values σ_i.

With the above condition number, equation (39), the sensitivity of solution to the wave decomposition step, equation (12) can be calculated for example. Letting $\alpha\rightarrow\infty$ in equation (39), the effect of perturbations, when only $\boldsymbol{p}$ is perturbed can be investigated. On the other hand when taking $\beta\rightarrow\infty$, the condition number reflects the sensitivity of the solution only to perturbations on $\boldsymbol{\Psi}$. By taking $\boldsymbol{L}$ as a column of the identity matrix, component wise condition numbers can be obtained, relating the sensitivity of specific components of $[\boldsymbol{p}^+\ \boldsymbol{p}^-]^T$ to perturbations of the data space for a specific choice of α and β.

Using the component wise condition numbers, it becomes possible to optimize the design of an experimental setup for certain specific conditions. For example if one is only interested in the behaviour of acoustic plane waves but needs accurate data for frequencies higher than the first cut-on frequency, the component wise condition numbers for the plane wave mode can be

optimized using a specific choice for $\boldsymbol{\Psi}$. As the partially condition numbers are computationally easy to compute, this choice can be obtained using numerical optimization techniques.

5. Results and discussion

In this section, results from the measurement of the reflection coefficient of a rigid wall will be presented. Two different experimental setups are used, one to determine the reflection coefficient using plane waves and the second where the reflection coefficients are determined for higher order modes. One advantage of using a rigid wall as the measurement object is that the acoustic impedance of the wall is homogeneous and there is no scattering of energy between different modes[34]. Therefore, only one acoustic field has to be measured to determine the reflection coefficient of each of the modes. This reduces the number of variables used in the computation significantly and it becomes easier to analyze the sources of the observed errors.

For the plane wave results, confidence intervals will be shown, obtained with the linear uncertainty analysis. The obtained covariance matrix from the linear uncertainty analysis will be compared against the covariance matrix obtained from a Monte-Carlo simulation. For the higher order modes, no bounds will be derived as it is shown that the linear uncertainty analysis is unsuitable to determine these bounds for the higher order mode reflection coefficients. The results from the higher order mode measurements show the presence of a random error in the obtained scattering coefficients and with the help of the perturbation theory, a plausible explanation is found for the observed scatter.

The basic construction of the two setups can be subdivided in three sections (see Figure 1). In the first section, the acoustic field is excited using loudspeakers that are flush mounted in the duct wall. In the second section, microphones flush mounted with the inner wall, measure the resulting sound field. The last section contains the device under study, which in this case is a rigid wall, mounted perpendicular to the duct axis. For each setup, the distances between the loudspeaker section, measurement section and the device under study are large enough, to ensure that non-propagating higher order modes do not contribute to the measured pressure at the microphone positions. No detailed information about the setups will be given, as the focus of the paper is on the use of methods to assess the measurement quality, but more information can be found in the cited references.

The first setup is used to measure within the plane wave range and it consists of a circular duct where one loudspeaker is attached to the wall of the duct to excite the sound field. The field is sampled by four microphones flush mounted in the side wall of the duct.[35] The second setup is designed to measure higher order modes and the waveguide has a rectangular cross-section. A combination of four loudspeakers is used to excite the sound field, with each wall of the duct having one loudspeaker. The sound field is measured with 20 flush mounted microphones located at various positions in the duct walls.[3,36]

To calculate the uncertainty in the reflection coefficients, the uncertainties on the measured parameters have to be known. For the sake of argument, only errors in the temperature T, acoustic pressures $\boldsymbol{p}$ and microphone distances x_i are considered, as these errors are the most significant.[35] In Table 1, the used uncertainties are given for two different cases. The uncertainties for the first case are based on experimental and technical information.[35] For the first case, the uncertainty in the temperature is taken to be 0.1°C, the uncertainty in the microphone position 0.1 mm and the uncertainty in the measured acoustic pressures to be normal circular distributed in the complex domain with a radius of 1% of the absolute value of the measured pressure. For the second case, the uncertainty of the microphone positions has been increased to 1 mm, to show non-linear error propagation. To assess the validity of the multi-variate analysis, the determinants of the covariance matrices obtained from the multi-variate analysis, $\det \Sigma_{\mathrm{MC}}$, are compared against the determinant obtained from the Monte-Carlo simulation, $\det \Sigma_{\mathrm{MVA}}$

$$\text{Covar ratio} \equiv \det \sum_{\mathrm{MC}} \Big/ \det \sum_{\mathrm{MVA}} - 1 \qquad (41)$$

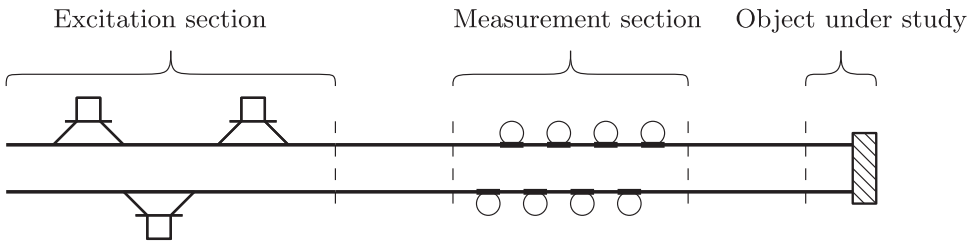

Figure 1. Schematic representation of the used measurement setups.

Table 1. Table of the standard deviation of the input variables for the two different cases.

		Case 1	Case 2
Temperature	[°C]	0.1	0.1
Distance	[mm]	0.1	1
Pressure	[Pa]	$\lvert p_i \rvert 10^{-3}$	$\lvert p_i \rvert 10^{-3}$

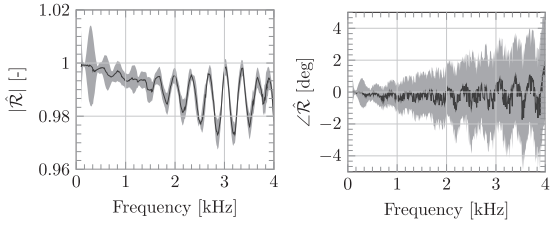

Figure 2. The measured reflection coefficient of the rigid plate (——) and the 95% confidence interval ( ).

This measure gives the relative difference in the size of the uncertainty region obtained from the two methods.

First the results in the plane wave region will be discussed. In Figure 2, the measured phase and magnitude of the reflection coefficient are shown together with the 95% confidence interval. It is customary to describe the scattering coefficients in polar form and the uncertainty can be expressed in a Cartesian reference frame, coinciding with the direction of the complex phasor defined by the reflection coefficient, by performing a transform on the covariance matrix.[37] When the uncertainties in the new Cartesian coordinate systems are small compared to the absolute value of the scattering coefficient, then the uncertainty can be expressed as uncertainties in phase and absolute value of the mean vector.[37]

Due to the linear nature of the analysis, equation (21), the total variance on the measurement is a superposition of the variances created by the individual uncertain inputs and the total variance can be analyzed to determine the sources that contribute the most to the overall error. In Figure 3, a breakdown of the variance is given for both the magnitude and the phase of the reflection coefficient. The errors contributing the most are different for the magnitude and phase. For the absolute value, the dominant factor is the uncertainty in the measured transfer functions. On the other hand, the uncertainty in the phase is dominated by the error related to the microphone positions and speed of sound.

In Figure 4, the ratio of the covariance matrices obtained for the reflection coefficient is shown for the

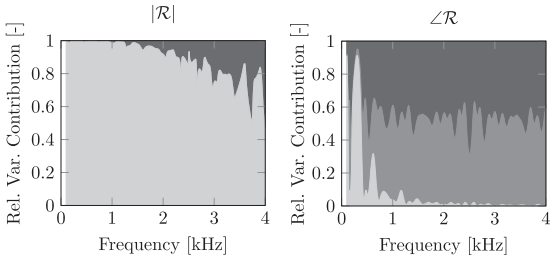

Figure 3. The relative contribution of each error source, microphone pressure ( ), temperature ( ) and microphone position ( ) to the variance of the error in the magnitude of the reflection coefficient (right) and the phase of the reflection coefficient (left).

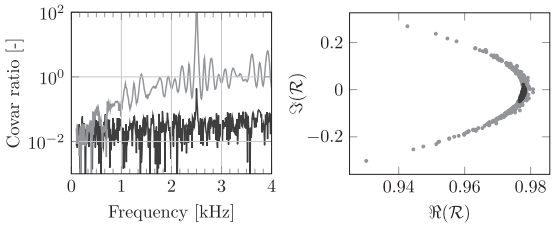

Figure 4. (Left) Relative difference between the determinant of the covariance matrix determined using the Monte-Carlo method and the linear multi-variate analysis as function of frequency. (Right) Scatter plot of the reflection coefficient at 2500 Hz calculated with the Monte-Carlo method for the two different cases. The different colors, (——,•) and (——,•) represent respectively Case 1 and Case 2 in Table 1.

two different sets of uncertainties given in Table 1. For the first case, the ratio is below 10% for most frequencies, showing that the linear analysis accurately describes the covariance matrix. The covariance ratio slowly increases with frequency, as the ratio between the second-order and first-order term of the Taylor expansion of Ψ increases with frequency.[30,32] On the other hand, for the second case, the covariance ratio is much larger, indicating that the linear analysis can not be used to determined the covariance matrix for the set of uncertainties. This is surprising, as even for the second case the ratios,[30,32] are met.

The obtained covariance matrices of the amplitudes p_1^+ and p_1^- for both the Monte-Carlo simulation and the linear analysis compare well to each other, with a maximum relative covariance ratio of 10 %, for both sets of uncertainties as could be expected from the linearity conditions. The source of non-linearity is the determination of the reflection coefficient from the wave amplitudes. The largest discrepancy is seen at 2500 Hz, and the obtained scatter plot of the Monte-Carlo simulation (Figure 4) shows the non-linear behaviour. The reason for this non-linear error propagation can be explained by considering the Taylor expansion of the reflection

coefficient with respect to the incident and reflected wave. The ratio between the second order terms to the first order terms is given by

$$\frac{1}{2}\frac{\epsilon^+}{p^+}\frac{\epsilon^- + \mathcal{R}\epsilon^+}{\epsilon^- - \mathcal{R}\epsilon^+} \tag{42}$$

If the errors on the incident and reflected pressure waves are almost equal, the linear terms, represented by the denominator in equation (42), cancel each other since $\mathcal{R} \approx 1$. When this happens, the error will propagate non-linearly even though that the overall error on the reflection coefficient can be small.

In the second part of this discussion, the focus is on the higher order modes. Because of the measurement object, there is no interaction between dissimilar modes and to calculate the scattering coefficients using equation (10), the information for each mode can be seen as a separate measurement. The matrix $\boldsymbol{P}^{\pm}$ can be written as a diagonal matrix, $\mathrm{diag}(p_1^{\pm}, \ldots, p_l^{\pm}, \ldots, p_L^{\pm})$ and the computed scattering matrix, will reduce to a diagonal matrix with the reflection coefficients of each mode on the diagonal.

In Figure 5, the reflection coefficient of the plane wave mode and the first higher order mode are shown for two different excitation configurations. For the first configuration, only one loudspeaker was used, situated on the top wall. For the second configuration, two loudspeakers mounted in the side walls and facing each other were used. Doak[38,39] investigated the excitation of higher order modes in rectangular ducts and showed that the excitation strength of the specific modes is sensitive to both the spatial distribution of the excitation sources and the end conditions of the duct. Therefore, the two different configurations lead to different amplitudes of the ingoing waves. From the reflection coefficients it can be seen that after the cut-on of the second higher order mode, the plane wave and first higher order mode reflection coefficients for the second configuration show more scatter compared to the results from the first configuration.

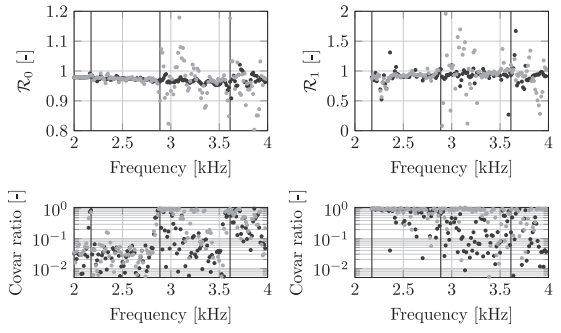

Figure 5. Reflection coefficient for the plane wave mode (left) and the first higher order mode (right) as function of frequency for two different acoustic excitations, case 1 (•) and case 2 (•). The vertical lines denote the cut-on frequencies of the higher order modes.

In the bottom row of Figure 5, the relative difference between the calculated covariance matrix for the reflection coefficient using the Monte-Carlo method and the multi-variate method is shown. The figure shows that after the second cut-on frequency, the covariance matrix for the plane waves is not correctly described by the linear analysis. The relative difference between the covariance matrices for the reflection coefficient for the first higher order mode is large for almost all frequencies, and the results obtained from the multivariate method cannot be used.

Similar to the results obtained for the plane wave case, the covariance matrices obtained for the individual travelling wave components with the two methods are in good agreement with each other below the third cut-on frequency except close to the cut-on frequencies. Here the covariance matrices obtained by the linear analysis and the Monte-Carlo simulation show larger differences as the condition number of $\boldsymbol{\Psi}$ is large, due to small wave number k_l for the cut-on higher order mode, in agreement with the condition (29).

The disparity between the covariance matrices of the reflection coefficients obtained by the linear method and the Monte-Carlo simulations is a consequence of the difference in magnitude of the individual wave components, which will be shown below. The difference in magnitude of the individual components leads to that the small components have a large relative error, which leads to non-linear error propagation to the scattering matrix due to the inversion step, equation (29), when determining the scattering matrix, equation (10).

In Figure 6, the condition number, based on perturbations of $\boldsymbol{p}$ for the individual wave components for the plane wave and first higher order mode are shown. For both the excitation cases, these graphs are identical, since $\boldsymbol{\Psi}$ is identical for the two cases. As the absolute value of the measured pressures for the two different cases has similar magnitudes, the induced error on the wave amplitudes is of a similar magnitude. It can be seen that the components of the first higher order mode, the sensitivity to errors on the measured pressures show a maximum at around 3000 Hz and that the results of the plane wave components are most sensitive to perturbations after the third cut-on frequency.

In the same figure, the second row depicts the condition number, based on perturbations of $\boldsymbol{\Psi}$. This condition number is similar for both cases, up to the cut-on of the second higher order mode, after which the condition numbers of the first configuration are higher than those of the second configuration. The errors on $\boldsymbol{\Psi}$ are identical as they are not dependent on the

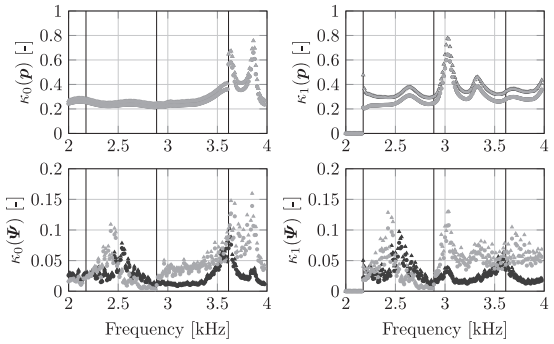

Figure 6. Partial condition numbers for the wave amplitudes of the plane wave mode (left column) and the first higher order mode (right column) as function of frequency for two different acoustic excitations. The top row denotes the partial condition numbers based on perturbations of the measured pressures $\boldsymbol{p}$, the bottom row shows the partial condition numbers based on perturbations of $\boldsymbol{\Psi}$. The positive travelling waves are denoted by triangles, (▲, ▲), and the negative travelling waves are denoted by circles, (●, ●), for respectively case 1 and case 2. The vertical lines denote the cut-on frequencies of the higher order modes.

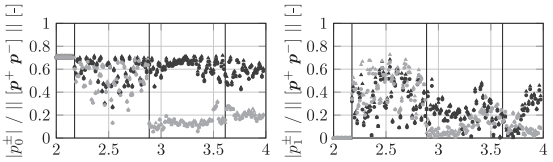

Figure 7. Relative size of the wave amplitudes of the plane wave mode (left column) and the first higher order mode (right column) as function of frequency for two different acoustic excitations. Triangles denote the positive traveling waves and circles the negative traveling waves. The vertical lines denote the cut-on frequencies of the higher order modes The positive travelling waves are denoted by triangles, (▲, ▲), and the negative travelling waves are denoted by circles, (●, ●), for respectively case 1 and case 2.

excitation conditions and thus the results for the first configurations are more sensitive to errors than for the second configuration, which correlates with the scatter on the measured scattering coefficients.

The main reason why the second configuration is more sensitive can be appreciated by looking at the relative size of the wave amplitudes compared to the solution vector. The relative size is depicted in Figure 7. It can be seen that for the second configuration, the relative amplitude of the plane wave and first-higher order mode are lower than those of the first excitation case after the cut-on of the second higher order mode and it correlates with the increased scatter on the measured results.

It is shown by Chandrasekaran and Ipsen[33] that the partial condition number of the solution components is inversely related to the relative size of the solution component to the size of the solution vector

$$K(p_l^{\pm}) \propto \frac{||\boldsymbol{p}^+ \boldsymbol{p}^-||}{|p_l^{\pm}|} \tag{43}$$

In this specific circumstance, the various modes do not interact with each other, because of the spatially uniform impedance that is being measured[34]. Furthermore, the presence of the wall determines the ratio between the amplitude of the in- and out- going wave for a specific mode and the relative size of the amplitudes of each of the modes is solely determined by the excitation and end conditions at the excitation side. To obtain reliable and repeatable results, independent of the object to be measured, the amplitudes of the ingoing wave components have to be controlled.

Another consequence of the large relative errors is that the resulting error on the reflection coefficient will depend non-linearly on the errors of the traveling wave amplitudes and a linear analysis cannot be used to determine the uncertainty in the scattering coefficients.

6. Conclusion

The validity of the linear uncertainty analysis to determine the uncertainty in the scattering matrix coefficients for higher order modes has been investigated. It has been shown that a linear multi-variate analysis can only be used in specific circumstances and conditions have been derived when such an analysis gives valid information on the uncertainty bounds for the wave decomposition method.

For higher order modes, the amount of conditions increases significantly and no general conditions can be formulated for when a linear uncertainty analysis can be used. Therefore, to determine accurate uncertainty intervals, a Monte-Carlo method has to be used. If the use of a Monte-Carlo method on the complete determination is too time consuming, a two step approach could be considered where the uncertainty in the wave decomposition is assessed with a linear analysis and the uncertainty in the scattering matrix determined using a Monte-Carlo methods.

The experimental results for the higher order mode scattering matrices have been analyzed with the help of the partial condition numbers. The partial condition numbers are a computational inexpensive alternative to investigate the problem and give qualitative information on the measurement quality. Using the partial condition numbers, it has been shown that the difference in excitation levels for each of the mode is the main reason for the large variance in the measured reflection coefficients. To reduce these errors, measurements have to performed where the energy in the modes can be controlled.

Acknowledgements

The presented work is part of the Marie Curie Initial Training Network Thermo-acoustic and Aero-acoustic Nonlinearities in Green combustors with Orifice structures (TANGO). The authors would like to thank Dr. Chenyang Weng for the helpful discussions.

Declaration of Conflicting Interests

The author(s) declared no potential conflicts of interest with respect to the research, authorship, and/or publication of this article.

Funding

The author(s) disclosed receipt of the following financial support for the research, authorship, and/or publication of this article: Luck Peerlings, Hans Bodén and Susann Boij gratefully acknowledge the financial support from the European Commission under call FP7-PEOPLE-ITN-2012.

ORCID iD

Luck Peerlings http://orcid.org/0000-0001-8099-6554.

References

1. Gerhold C, Cabell R and Brown M. Development of an experimental rig for investigation of higher order modes in ducts. In: *12th AIAA/CEAS Aeroacoustics conference*. Cambridge, US: American Institute of Aeronautics and Astronautics (AIAA), 2006.
2. Sack S, Åbom M, Schram CF, et al. Generation and scattering of acoustic modes in ducts with flow. In: *20th AIAA/CEAS Aeroacoustics conference,* 2014.
3. Weng C, Otto C, Peerlings L, et al. Experimental investigation of sound field decomposition with higher order modes in rectangular ducts. In: *22nd AIAA/CEAS Aeroacoustics conference*. Lyon, France: American Institute of Aeronautics and Astronautics (AIAA), 2016.
4. Weng C. *Modeling of sound-turbulence interaction in low mach number duct flows*. Licentiate thesis, KTH Royal Institute of Technology, Stockholm, Sweden, 2013.
5. Åbom M and Bodén H. Error analysis of two-microphone measurements in ducts with flow. *J Acoust Soc Am* 1988; 83: 2429–2438.
6. Bodén H. Influence of errors on the two-microphone method for measuring acoustic properties in ducts. *J Acoust Soc Am* 1986; 79: 541–549.
7. Hudde H and Letens U. Untersuchung zum akustischen meßleitungsverfahren mit festen meßorten. *Acustica* 1984; 56: 258–268.
8. Katz BFG. Acoustic absorption measurement of human hair and skin within the audible frequency range. *J Acoust Soc Am* 2000; 108: 2238–2242.
9. Boonen R, Sas P, Desmet W, et al. Calibration of the two microphone transfer function method with hard wall impedance measurements at different reference sections. *Mech Syst Signal Process* 2009; 23: 1662–1671.
10. Dickens P, Smith J and Wolfe J. Improved precision in measurements of acoustic impedance spectra using resonance-free calibration loads and controlled error distribution. *J Acoust Soc Am* 2007; 121: 1471–1481.
11. Gibiat V and Laloë F. Acoustical impedance measuremetns using the two microphone three calibration method. *J Acoust Soc Am* 1990; 88: 2533.
12. Schultz T, Sheplak M and Cattafesta L. Uncertainty analysis of the two-microphone method. *J Sound Vibrat* 2007; 304: 91–100.
13. Sack S and Åbom M. On acoustic multi-port characterisation including higher order modes. *Acta Acustica United with Acustica* 2016; 102: 834–850.
14. Suzuki T and Day BJ. Comparative study on mode-identification algorithms using a phased-array system in a rectangular duct. *J Sound Vibrat* 2015; 347: 27–45.
15. Coleman HW and Steele WG. *Experimentation, validation, and uncertainty analysis for engineers*. Hoboken, New Jersey, US: John Wiley & Sons, Inc, 2009.
16. Lavrentjev J and Åbom M. Characterization of fluid machines as acoustic multi-port source. *J Sound Vibrat* 1996; 197: 1–16.
17. Marks R and Williams D. A general waveguide circuit theory. *J Res Natl Inst Stand Technol* 1992; 97: 533–562.
18. Kuh ES and Rohrer R. *Theory of linear active networks*. San Fransisco, US: Holden-Day Inc., 1967.
19. Eriksson LJ. Higher order mode effects in circular ducts and expansion chambers. *J Acoust Soc Am* 1980; 68: 545–550.
20. Weng C, Boij S and Hanifi A. On the calculation of the complex wavenumber of plane waves in rigid-walled low-mach-number turbulent pipe flows. *J Sound Vibrat* 2015; 354: 132–153.
21. Weng C and Bake F. An analytical model for boundary layer attenuation of acoustic modes in rigid circular ducts with uniform flow. *Acta Acustica united with Acustica* 2016; 102: 1138–1141.
22. Beatty RE. Boundary layer attenuation of higher order modes in rectangular and circular tubes. *J Acoust Soc Am* 1950; 22: 850–854.
23. Johnson RA and Wichern DW. *Applied multivariate statistical analysis*. New Jersey, United States: Prentice-Hall. ISBN 0-13-041807-2, 1992.
24. Schreier PJ and Scharf LL. *Statistical Signal Processing of Complex-Valued Data*. Cambridge, England: Cambridge University Press. ISBN 978-0-511-81591-1, 2010.
25. Anderson TV and Mattson CA. Propagating skewness and kurtosis through engineering models for low-cost, meaningful, nondeterministic design. *J Mech Design* 2012; 134: 100911.
26. Stewart GW and Sun JG. *Matrix perturbation theory*. Boston, US: Academic Pr Inc, 1990. ISBN 0-12-670230-6.
27. Deif A. *Sensitivity analysis in linear systems*. Berlin, Germany: Springer, 1986. ISBN 3-642-82741-1.
28. Geurts AJ. A contribution to the theory of condition. *Numerische Mathematik* 1982; 39: 85–96.
29. Arioli M, Baboulin M and Gratton S. A partial condition number for linear least squares problems. *SIAM J Matrix Anal Appl* 2007; 29: 413–433.

30. Baboulin M, Dongarra J, Gratton S, et al. Computing the conditioning of the components of a linear least-squares solution. *Num Linear Algebra Appl* 2009; 16: 517–533.
31. Gratton S. On the condition number of linear least squares problems in a weighted frobenius norm. *BIT Num Math* 1996; 36: 523–530.
32. Åke Wedin P. Perturbation theory for pseudo-inverses. *BIT* 1973; 13: 217–232.
33. Chandrasekaran S and Ipsen I. On the sensitivity of solution components in linear systems of equations. *SIAM J Matrix Anal Appl* 1995; 16: 93–112.
34. Morse PM and Ingard KU. *Theoretical acoustics*. Princeton, New Jersey, US: Princeton University Press, 1987. ISBN 0-691-02401-4..
35. Peerlings L. *Methods and techniques for precise and accurate in-duct aero-acoustic measurements*. Licentiate thesis, Stockholm, Sweden: KTH Royal Institute of Technology, 2015.
36. Busse-Gerstengarbe S, Bake F, Enghardt L, et al. Comparative study of impedance eduction methods, part 1: DLR tests and methodology. In: *19th AIAA/CEAS Aeroacoustics Conference*. Berlin, Germany: American Institute of Aeronautics and Astronautics (AIAA).
37. Williams DF, Wang CM and Arz U. In-phase/quadrature covariance-matrix representation of the uncertainty of vectors and complex numbers. *2006 68th ARFTG Conference: Microwave Measurement*, Broomfield, Colorado, United States, 2006, pp.1–4.
38. Doak P. Excitation, transmission and radiation of sound from source distributions in hard-walled ducts of finite length (i): the effects of duct cross-section geometry and source distribution space-time pattern. *J Sound Vibrat* 1973; 31: 1–72.
39. Doak P. Excitation, transmission and radiation of sound from source distributions in hard-walled ducts of finite length (ii): the effects of duct length. *J Sound Vibrat* 1973; 31: 137–174.